

Article

Not peer-reviewed version

---

# First-Principles Study on Silicon Stabilization of the Cubic $\alpha$ - and Hexagonal $\alpha'$ -FeAl Phases

---

[Changming Fang](#)\*, [Zhongping Que](#), [Zhongyun Fan](#)

Posted Date: 15 May 2026

doi: 10.20944/preprints202605.1023.v1

Keywords: Si stabilization; Fe-containing intermetallic compounds; cubic  $\alpha$ -phase; hexagonal  $\alpha'$  phase; first-principles calculations; density-functional theory



Preprints.org is a free multidisciplinary platform providing preprint service that is dedicated to making early versions of research outputs permanently available and citable. Preprints posted at Preprints.org appear in Web of Science, Crossref, Google Scholar, Scilit, Europe PMC, OpenAlex.

Copyright: This open access article is published under a [Creative Commons CC BY 4.0 license](#), which permit the free download, distribution, and reuse, provided that the author and preprint are cited in any reuse.

Disclaimer/Publisher's Note: The statements, opinions, and data contained in all publications are solely those of the individual author(s) and contributor(s) and not of MDPI and/or the editor(s). MDPI and/or the editor(s) disclaim responsibility for any injury to people or property resulting from any ideas, methods, instructions, or products referred to in the content.

Article

# First-Principles Study on Silicon Stabilization of the Cubic $\alpha$ - and Hexagonal $\alpha'$ -FeAl Phases

Changming Fang \*, Zhongping Que and Zhongyun Fan

Brunel Centre of Advanced Solidification Technology (BCAST), Brunel University London, Uxbridge UB8 3PH, The United Kingdom (UK)

\* Correspondence: changming.fang1@brunel.ac.uk

## Abstract

Commercial aluminum (Al) metals contain unavoidably iron (Fe) and silicon (Si) as impurities. Due to its low solubility and high chemical affinity to Al, Fe exists in the form of Fe-containing intermetallic compounds (Fe-IMCs) which act crucially in solidification processes, determining the micro-structure and consequently the mechanical performance of the cast parts. Meanwhile, Si as impurity or addition may join the binary Fe-IMCs. Here, we investigate the Si stabilization effects on the frequently observed Al-rich Fe-IMCs in a comprehensive and systematic way using a first-principles density-functional theory (DFT) approach. The study revealed different Si stabilization effects on the cubic  $\alpha$ - and hexagonal  $\alpha'$ -phase, as well as other binaries:  $\text{Al}_{12}\text{Fe}$ ,  $\eta\text{-Al}_6\text{Fe}$ ,  $\tau_4$ ,  $\beta$ - and  $\theta$ -phases. The enhancement of stability for the  $\alpha$ -phase is moderate while it is strong for the  $\alpha'$ -phase. For the stability series (from higher to lower) is  $\theta\text{-Al}_{13}\text{Fe}_4 > \eta\text{-Al}_6\text{Fe} > \alpha\text{-Al}_{4.75}\text{Fe}$  in the binary system, while it becomes  $\tau_4\text{-(Al,Si)}_5\text{Fe} > \beta\text{-Al}_{4.5}\text{SiFe} > \alpha'\text{-(Al,Si)}_{4.174}\text{Fe}$  for the ternary Fe-IMCs. The information obtained here helps understand the formation of Fe-IMCs particles during casting of Al-Si alloys, and design of novel Al alloys of fine micro-structures and desired mechanical performances of the products from the primary Al and the scraps and wastes.

**Keywords:** Si stabilization; Fe-containing intermetallic compounds; cubic  $\alpha$ -phase; hexagonal  $\alpha'$ -phase; first-principles calculations; density-functional theory

## 1. Introduction

Commercial Al metals contain unavoidably impurities including iron (Fe) and silicon (Si). The low solid solubility of Fe (less than 0.05wt.%) at equilibrium in solid Al and its high affinity to Al [1,2] drive it to form Fe-containing intermetallic compounds (Fe-IMCs) in aluminium-based alloys [2,3]. Si is frequently added to Al metals for improving castability, refining microstructures and enhancing mechanical properties of the cast parts [3,4]. The Si impurity or addition may adjoin the binary AlFe compounds to produce ternary Fe-IMCs. The Fe-IMCs particles formed during casting exhibit various morphologies and may deteriorate the mechanical performance of the products. Such deterioration effect becomes more severe for recycling of Al scraps/wastes in which various Fe-IMCs particles would have been accumulated during usage, storage and treatments [5–8]. Various methods including separating the heavier Fe-IMCs particles from the liquids [9,10], manipulating solidification processes and/or adding minor elements to transform the detrimental Fe-IMCs into less harmful or even beneficial nano-sized particles [11–14] have been explored. Reaching such aims means demanding for a systematic and comprehensive understanding about the crystal chemistry of the Al-rich Fe-IMCs, which helps manipulate the formation of the Fe-IMCs in various Al ingots including Al-scraps/wastes which contain various contents of Fe and Si [1,10,11]. The latter is important for our environment and the increasingly important recycling economy [15–17].

Currently, experiments focus on alloy manufacturing, micro-structural analysis, phase characterizations [1–4,7,9,12–14,18–21] and mechanical properties measurements [21–23]. Moreover, great efforts have been made to determine the crystal structures of these Al-rich Fe-IMCs. Structural

models were built for the  $\eta$ -Al<sub>6</sub>Fe [24],  $\tau_4$ - [25,26],  $\beta$ - [27–29], cubic  $\alpha$ - [30], hexagonal  $\alpha'$ - [31,32], and  $\theta$ -phase [33] based on dominantly X-ray-diffraction patterns and structural refinements. For most ternary Fe-IMCs, the structural determination generally provided ‘averaged’ patterns that the Al/Si atoms were assumed to be uniformly distributed at the Wyckoff sites of the Al atoms. One example is in the cubic  $\alpha$ -(AlFeSi) phase [30]. Moreover, there are partial atomic occupations at the specific Wyckoff sites in, *e.g.* the hexagonal  $\alpha'$ -(AlFeSi) phase [31,32]. Al/Si distribution often complicates our understanding about their thermodynamic properties under solidification conditions and the mechanical performance of the produced alloys in practice.

In this respect, atomistic modeling methods, particularly parameter-free *ab initio*/first-principles approaches become helpful. First-principles approaches can assist in building structural models and predicting intrinsic structural properties for complex compounds [34,35]. First-principles’ density-functional theory (DFT) approaches have been applied to the Fe-IMCs related materials [36–44]. Wolverton and Ozolins [36] constructed an energetic database for a series of binary Al-containing alloys and compounds including several Fe-IMCs with the help of DFT methods. Liu, *et al.* reported the results of their first-principles study on the mechanical properties and electronic structures of several binary Fe-IMCs [37]. The Al/Si ordering in the  $\beta$ -AlFeSi phase was investigated using an electronic DFT method [38,39]. Popčević, *et al.* investigated the electronic and magnetic properties of  $\theta$ -Al<sub>13</sub>Fe<sub>4</sub> phase [40]. Ma studied the mechanical and electronic properties of  $\alpha$ -AlMnSi [41]. Zhang, *et al.* performed first-principles modelling on the Fe/Mn occupation in  $\alpha$ -AlMnFeSi [42]. Amirkhanyan, *et al.* studied the stability and lattice vibrations of the  $\tau_4$ -phase [43]. Si occupation at the Al sites in the Fe-IMCs including  $\eta$ -Al<sub>6</sub>(Mn,Fe) alloying phase [44],  $\beta$ - [45],  $\tau_4$ -phase [46] and  $\theta$ -Al<sub>13</sub>Fe<sub>4</sub> [44,47,48], as well as the cubic  $\alpha$ -Al(Fe,Mn) phase [49] was investigated by means of first-principles tools. Meanwhile, there is still a lack of comprehensive understanding about structural models and Si occupations in the ternary cubic  $\alpha$ - and hexagonal  $\alpha'$ -phase, together with other binary Fe-IMCs. We here investigate the structure chemistry of the binary  $\alpha$ - and  $\alpha'$ -phase starting from the available experimental models [30–32]. This study also includes the Si stabilization effects on other frequently observed Fe-IMCs, (novel) Al<sub>12</sub>Fe,  $\eta$ -Al<sub>6</sub>Fe,  $\tau_4$ -(Al,Si)<sub>5</sub>Fe,  $\beta$ -Al<sub>4.5</sub>SiFe and  $\theta$ -(Al,Si)<sub>13</sub>Fe<sub>4</sub> phases. This produces a systematic and comprehensive understanding about their stability and the related Si stabilization effects on these Al-rich Fe-IMCs. The information obtained here is useful to design new casting processes and new Al alloys from both primary Al billets and scraps/wastes.

## 2. Methods

The stability of one Fe-IMC with the chemical formula Al<sub>k</sub>Si<sub>m</sub>Fe<sub>n</sub>, can be referred to the related elemental solids. Therefore, its formation energy ( $\Delta E_f$ ) is defined as:

$$\Delta E_f(\text{Al}_k\text{Si}_m\text{Fe}_n) = \{E(\text{Al}_k\text{Si}_m\text{Fe}_n) - [k E(\text{Al}) + m E(\text{Si}) + n E(\text{Fe})]\}/n \quad (1)$$

Here,  $E(\text{Al}_k\text{Si}_m\text{Fe}_n)$ ,  $E(\text{Al})$ ,  $E(\text{Si})$  and  $E(\text{Fe})$  represent the calculated total valence-electrons energies for Al<sub>k</sub>Si<sub>m</sub>Fe<sub>n</sub> and the elemental solids,  $\alpha$ -Al, Si and  $\alpha$ -Fe, respectively. The unit of the formation energy,  $\Delta E_f$  is eV per Fe atom.

In order to assess the Si stabilisation effects to the binary Fe-IMCs, the formation energy of the Si adjoined the compound Al<sub>k</sub>Si<sub>m</sub>Fe<sub>n</sub> in its unit cell is defined as:

$$\Delta E_{Si}(\text{Al}_k\text{Si}_m\text{Fe}_n) = E(\text{Al}_k\text{Si}_m\text{Fe}_n) - \{E(\text{Al}_{(k+m)}\text{Fe}_n) + m [(E(\text{Si}) - E(\text{Al}))]\} \quad (2)$$

Here,  $E(\text{Al}_{(k+m)}\text{Fe}_n)$  represents the total valence-electrons energy for Al<sub>(k+m)</sub>Fe<sub>n</sub>. The unit of formation energy in Equation 2 is eV per cell.

Considering the Fe-IMCs with various Al(Si)/Fe ratios, the formation energy of a Si adjoined compound Al<sub>k</sub>Si<sub>m</sub>Fe<sub>n</sub> is unified into eV/Fe as following,

$$\Delta E_{Si2}(\text{Al}_k\text{Si}_m\text{Fe}_n) = \Delta E_{Si}(\text{Al}_k\text{Si}_m\text{Fe}_n)/n \quad (3)$$

A negative value of the formation energy in the Equations means that the reaction is exothermal and the formation of the compound is favored.

The first-principles' Vienna *Ab initio* Simulation Package (VASP) [50] was employed in the present study. This code utilizes the Density-Functional Theory (DFT) [51] within the projector-augmented wave (PAW) method [52]. The spin-polarized generalized gradient approximation (GGA) formulated by Perdew, Burke and Ernzerhof (PBE) [53] was used for the exchange and correlation energy terms, as the GGAs describe the 3d metals including Fe and related compounds better than the standard local (spin-polarized) density approximation [53,54].

The cut-off energies for the wave functions and for the augmentation functions were set to be 550.0eV and 700.0eV, respectively. These cut-off energies are notably higher than the default values ( $E_{MAX}/E_{AUG} = 245.3 \text{ eV}/322.1 \text{ eV}$  for Si,  $240.3 \text{ eV}/291.1 \text{ eV}$  for Al, and  $267.9 \text{ eV}/511.4 \text{ eV}$  for Fe, respectively) in the atomic pseudo-potentials. The electronic wave functions were sampled densely on *e.g.* a  $6 \times 6 \times 6$  grid with 11 to 108 *k*-points in the irreducible Brillouin zones of the cubic  $\alpha$ -(Si<sub>1-x</sub>Al<sub>x</sub>)<sub>114</sub>Fe<sub>24</sub> phase, depending on the symmetry using the Monkhorst-Pack method [55]. Structural optimizations were performed for both lattice parameters and coordinates of atoms. Different *k*-meshes and cut-off energies were tested, which showed a good convergence with deviations within 1 meV/atom.

### 3. Results

First-principles structural optimizations were first performed for the related elemental solids, Al, Si and Fe, all of them have cubic lattices. The calculations produced a lattice parameter of 4.039Å (4.0493Å) for  $\alpha$ -Al, 5.468Å (5.431Å) for Si and 2.829Å (2.8665Å) for  $\alpha$ -Fe. These calculated values agree well with the experimental data at room temperature [56] (see the values in the parenthesis). The calculations provided a ferromagnetic solution for  $\alpha$ -Fe which atom contains 3d<sup>6</sup> electrons. The obtained local moment is moderate (2.17 $\mu_B$ /Fe) which is close to the experimental value (2.22 $\mu_B$ /Fe) [57]. The excellent agreements between the experimental measured values and the calculations mean availability of this approach and the settings.

The calculations also showed that Fe solution in Al matrix, which was modelled in a  $3a_0 \times 3a_0 \times 3a_0$  supercell,  $a_0$  being the lattice of Al and thus the formula was Al<sub>107</sub>X, X = Fe or Si) is favored with the formation energy of -0.45eV/Fe. Meanwhile solution of Si in the Al matrix costs energy (+0.43eV/Si) (Table 1). The bond lengths between the impurities and the surrounding Al atoms are 2.74Å (Fe-Al) and 2.84Å (Si-Al), respectively. These values are shorter than the Al-Al bond (2.86Å) in  $\alpha$ -Al.

**Table 1.** The calculations for the binary  $\alpha$ - (cubic) and  $\alpha'$ -AlFe (hexagonal) models based on the experimental determinations which values are in the parenthesis [30] or specifically labeled [31,32]. FCC/BCC represents face-centered cubic/body-centered cubic. The unit of the dilute Fe in Al matrix and the formation energies of the compounds,  $\Delta E_{fj}$  is eV/Fe via Equation 1.

Phase	Lattice/space group	Latt. paras.(Å)	$E_{val.-elect.}$	Remark
A. Solute Fe and Si in Al matrix				
Al <sub>107</sub> Fe	-	-	-0.449(eV/Fe)	d(Fe-Al):2.74Å(×12)
Al <sub>107</sub> Si	-	-	+0.431(eV/Si)	d(Si-Al): 2.84Å(×12)
B. Cubic $\alpha$ -AlFe with space group P-3m (200) Cooper [30]				
$\alpha$ -Al <sub>114</sub> Fe <sub>24</sub>	Cub. PM-3 (No. 200)	$a = 12.622(12.56)$ [30]	-1.315(eV/Fe)	Based on [30]
C. Hexagonal $\alpha'$ -AlFe with space group P6 <sub>3</sub> /mmc (194), 607475-ICSD, Corby-Black [31]				
Config-1 Al <sub>194</sub> Fe <sub>46</sub>	Hex./P6 <sub>3</sub> /mmc (194)	$a = 12.450(\text{Å})$ $c = 26.393(\text{Å})$	-1.301(eV/Fe)	Al17 are removed
Config-2 Al <sub>192</sub> Fe <sub>46</sub>	Hex./P6 <sub>3</sub> /mmc (194)	$a = 12.446(\text{Å})$ $c = 26.374(\text{Å})$	-1.289(eV/Fe)	Al17 and Al18 are removed
Config-3 Al <sub>188</sub> Fe <sub>46</sub>	Hex./P6 <sub>3</sub> /mmc (194)	$a = 12.380(\text{Å})$ $c = 26.349(\text{Å})$	-1.239(eV/Fe)	Al17 and Al14 are removed
Config-4 Al <sub>186</sub> Fe <sub>46</sub>	Hex./P6 <sub>3</sub> /mmc (194)	$a = 12.379(\text{Å})$ $c = 26.225(\text{Å})$	-1.250(eV/Fe)	Al17, Al14 and Al18 are removed
Exper. Al <sub>192-194</sub> Fe <sub>46</sub>	Hex./P6 <sub>3</sub> /mmc (194)	$a = 12.404(\text{Å})$ [31] $c = 26.234(\text{Å})$ [31]	-	Al16/Al17 mixing, Al18 small occup.

$a = 12.3445(\text{\AA})$ [32]	Symmetry of the crystal is broken.
$c = 26.210(\text{\AA})$ [32]	

### 3.1. Structure of the Binary $\alpha$ - and $\alpha'$ -AlFe Phases

Cooper determined the crystal structure of the cubic  $\alpha$ -(AlFeSi) crystals which contained an amount of Mn [30]. He proposed three models with fully Al occupied Wyckoff sites, based on the X-ray diffractions patterns. The models avoid partial occupations and keep the symmetry of the systems [30]. Structural refinements provided similar values of refinement goodness for the three models. The atomic coordinates and related occupations for Model 3 in [30] are listed in the supplementary Materials (Table S-1) with the labels of the atom species. The unit cell contains 138 atoms with chemical formula  $\text{Al}_{114}\text{Fe}_{24}$ .

First-principles calculations were performed for the three models and revealed similar formation energies. The results of structure optimisations for the cubic  $\alpha$ -AlFe phase (Model 3) are shown in Table 1.

The crystal structure of the hexagonal  $\alpha'$ -(AlFeSi) phase was experimentally investigated for long [31,32,58]. Corby and Black determined the crystal structure of the hexagonal  $\alpha'$ -(AlFeSi) phase by means of the anomalous-dispersion methods with three different wavelengths of radiation on a single-crystal [31]. The crystal structure of  $\alpha'$ -(AlFeSi) has a space group of  $P6_3/mmc$  (194) and lattice parameters,  $a = 12.404(\text{\AA})$  and  $c = 26.234(\text{\AA})$  [31]. There are 23 different atomic species, five Fe and 18 Al. The Si atoms were assumed to be homogeneously distributed at the Al sites. There are partial occupations at the Al/Si sites [31]. Roger *et al* [32] refined the crystal structure of  $\alpha'$ -(AlFeSi) and obtained lattice parameters slightly different from those in [31], as shown in Table 1. Moreover, the Al and Si separately occupied sites were reported [32]. The atomic coordinates and related occupations are listed in the Supplementary Materials, Table S-2 for both the Corby-Black model [31] and the Roger-model (CSD-422224) [32]. Table S-2 also includes the labels of the atom species. If we take full occupation of all Al sites, the chemical formula is  $\alpha'$ - $\text{Al}_{200}\text{Fe}_{46}$ . However, this model contains short interatomic distances between Al16 and Al(Si)17 with short Al-Al(Si) distance ( $<0.5\text{\AA}$ ), which means partial occupation at the two sites. Therefore, occupation of either Al16 or Al17 should be chosen to keep the system symmetry. Moreover, the occupation of Al(Si)18 (2c) sites is small (0.14 [32] or 0.29 [31]). The experimental structural model is 'averaged' and the symmetry is practically broken.

Based on the structural model [31,32], we performed first-principles calculations for configurations with Al vacancies at the Al sites and found the ones with low energy costs as shown in Table 1. We calculated configurations with Al vacancy either at Al16 or Al17 sites and revealed the same formation energy. The results for one vacancy at the Al17 sites with the chemical formula  $\text{Al}_{194}\text{Fe}_{46}$  for the configurations were shown in Table 1.

As shown in Table 1, the calculated lattice parameter for the cubic  $\alpha$ - $\text{Al}_{114}\text{Fe}_{24}$  is  $12.622\text{\AA}$  which is close to the experimental value for the ternary compound ( $12.56\text{\AA}$ )[30]. The calculated formation energy is  $-1315\text{meV/Fe}$ .

The hexagonal  $\alpha'$ -phase with the maximum Al content has the chemical formula  $\text{Al}_{194}\text{Fe}_{46}$  (Config-1 in Table 1) with a formation energy of  $-1301\text{meV/Fe}$ . This  $\alpha'$ - $\text{Al}_{194}\text{Fe}_{46}$  is obtained by removing either the Al16 or Al17 atoms. We also performed structural optimizations and total energy calculations for configurations with Al vacancies at mixing Al16/Al17, in which systems the symmetry is broken. The calculations produced the same formation energy within the numeric errors as that of Config-1.

Decreasing the number of Al atoms in unit cell of  $\alpha'$ -phase induces increasing of the formation energies (Table 1). When both 1 atoms at Al17 and Al18 atoms were removed, the formation energy of  $\alpha'$ -( $\text{Al}_{1-x}\text{Si}_x$ ) $_{192}\text{FeSi}_{46}$  (Config-2) is  $-1289\text{meV/Fe}$ , just slightly lower than that of Conf-1. This configuration was selected for the study of Si stabilization effect, considering the moderate occupation at Al(Si)18 [31,32]. Further removing Al atoms at other sites, *e.g.* Al14 causes notably decreasing of the stability of the systems.

### 3.2. Si Stabilization Effect on the Cubic $\alpha$ -FeAl<sub>4.75</sub> Phase

Table 1 showed that the crystal structure of the  $\alpha$ -(AlFeSi) phase has a cubic lattice (space group Pm-3, Nr. 200) [30]. There are two types of iron species which are labelled as Fe1 at 12j and Fe2 at 12k Wyckoff sites and nine Al species at the 6e (Al1), 6h (Al2), 12j (Al3), 12k (Al4), 24 l (Al5), 24l (Al6), 6f (Al7), 12j (Al8) and 12k (Al9) (Table S-1). All the sites have full occupation with the chemical formula Al<sub>14</sub>Fe<sub>24</sub>. The Si content was not determined using the X-ray diffraction method and the Si atoms were assumed to be uniformly distributed at the Al sites [30].

To obtain detailed information about Si effects at the Al sites, we used two kinds of Si replacements of the Al atoms. One is using the configurations with one Si replacing one Al at each of the nine Al sites. These configurations lose their symmetry. Another one is full replacement of Al by Si at each Al site, keeping the system symmetry. The results are listed in Table 2.

The calculations revealed a rich variety of Si stabilization effects on the Al sites. There are three different types of consequences of Si doping at the Al sites (Table 2): high energy costs ( $\Delta E_{Si} \sim 0.5\text{eV/Si}$ ) for one Si atoms to replace one Al at the Al1, Al2, Al5, Al6 and Al9 sites; a moderate energy cost (0.26eV/Si) for the Al8 and negative formation energies for one Si atoms at the Al3 (-0.06eV/Si), Al4 (-0.28eV/Si) and Al7 (-0.001eV/Si). Interestingly, the formation energy of the system increases with increasing Si content and to maximum when full occupation at the Al7 sites. At the same time, low Si occupation at both Al3 and Al4 sites has negative formation energies, whereas the formation energies become positive with high Si occupations. The relations between the formation energies and Si content at the Al3, Al4, and Al7 were shown in Figure 1a with the formation energies being obtained according to Equation 3 with the unit meV/Fe.

The formation energy ( $\Delta E_{Si}$ ) decreases with Si content increases at the Al7 sites and reached minimum at the full occupation ( $\Delta E_{Si} = -0.28\text{eV/cell}$ ) (Table 2). It decreases with Si content up to about one quarter occupation at the Al3 sites with formation energy,  $\Delta E_{Si}$  being -0.15eV/cell. It is notable that Si occupation at five of the twelve Al4 sites has the lowest formation energy,  $\Delta E_{Si} = -0.95\text{eV/cell}$  or -40meV/Fe in Figure 1a.

**Table 2.** The calculated results (lattice parameters, coordination numbers of Si and formation energies via Equations 1, ( $\Delta E_{Fe}$ ) and 2, ( $\Delta E_{Si}$ ) for configurations with 1Si or full occupation at the Al sites. The bond-lengths were chosen to be shorter than 3.0Å. The unit of formation energies,  $\Delta E_{Fe}$  is eV/Fe according to Equation 1 and  $\Delta E_{Si}$  is eV/(cell) according to Equation 2, respectively.

Si at Al sites	Latt.params.(Å) & Vol. (Å <sup>3</sup> /cell)				Local coordination of Si by Fe/Mn	$\Delta E_{Fe}$ (eV/Fe)/ $\Delta E_{Si}$ (eV/(cell))
	a	b	c;	V		
Al <sub>14</sub> Fe <sub>24</sub>	12.622, 12.622, 12.622,	2011.06			-	-1.315/0
6Si at Al1	12.590, 12.590, 12.590;	1995.53			Si have two Fe and ten Al.	-1.169/+3.501
1Si1	12.595, 12.626, 12.623;	2007.45			Si1 has two Fe and ten Al.	~/+0.596
6Si at Al2	12.603, 12.603, 12.603;	2001.68			Si have two Fe, one Si and 12 Al.	-1.133/+4.267
1Si2	12.600, 12.634, 12.629;	2010.32			Si2 has two Fe and 11 Al.	~/+0.697
12Si at Al3	12.570, 12.570, 12.570;	1986.08			Si have one Fe, five Si and five Al.	-0.234/+3.469
1Si3	12.612, 12.619, 12.626;	2009.35			Si1 has one Fe and ten Al.	~/ <b>-0.064</b>
12Si at Al4	12.553, 12.553, 12.553;	1978.30			Si have one Fe, five Si and five Al.	-0.326/+1.260
1Si4	12.606, 12.612, 12.620;	2006.31			Si1 has one Fe and ten Al.	~/ <b>-0.278</b>
24Si at Al5	12.635, 12.635, 12.635;	2017.15			Si have two Fe and nine Al.	-0.770/0.668
1Si5	12.620, 12.613, 12.619;	2008.57			Si have three Fe and nine Al.	~/+0.498
24Si at Al6	12.637, 12.637, 12.637;	2017.89			Si have two Fe and nine Al.	-0.770/+0.668
1Si6	12.626, 12.667, 12.621;	2018.55			Si have three Fe and nine Al.	~/+0.498
6Si at Al7	12.587, 12.587, 12.587;	1993.96			Si have two Fe and ten Al	-1.327/ <b>-0.283</b>
1Si7	12.623, 12.636, 12.594;	2008.78			Si1 has two Fe and eight Al With a long Fe-Al bond (~3.01Å)	~/ <b>-0.001</b>
12Si at Al8	12.547, 12.547, 12.547;	1975.02			Si have three Fe, one Si and 7 Al.	-0.241/+0.275
1Si8	12.627, 12.610, 12.609;	2007.73			Si8 has three Fe and eight Al.	~/+0.257

12Si at Al9	12.567, 12.567, 12.567; 1984.85	Si have two Fe, one Si and six Al	-0.122/0.514
1Si9	12.612, 12.617, 12.615; 2007.49	Si1 has two Fe and seven Al.	~+/0.487

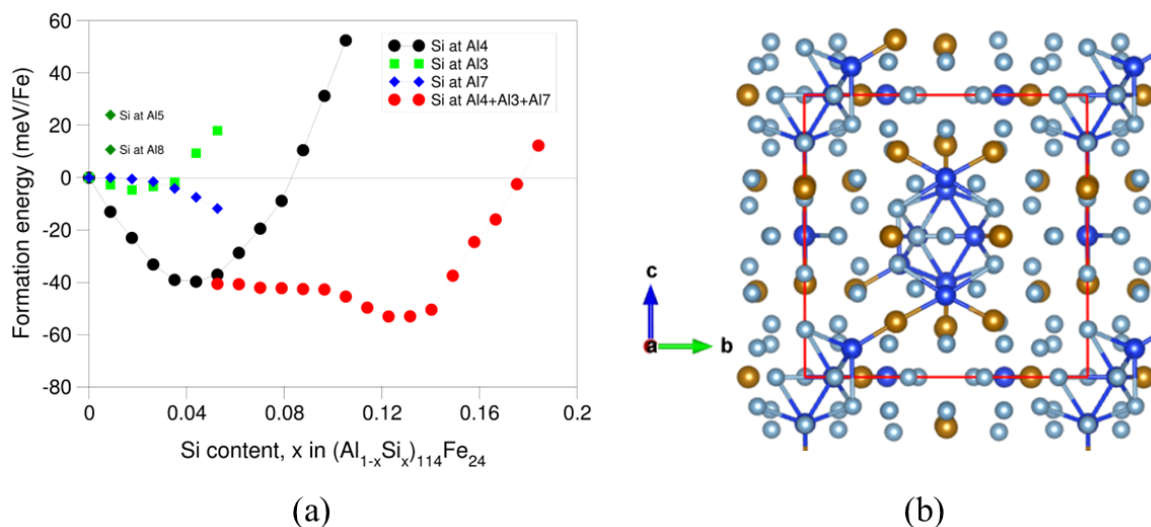


**Figure 1.** (b) The schematic structure of  $\alpha-(Al_{0.8772}Si_{0.1228})_{114}Fe_{24}$  and (a) calculated relationship between the formation energy and the Si content for the highly stable configurations of the cubic  $\alpha-(Al_{1-x}Si_x)_{114}Fe_{24}$  ( $\Delta E_{Si2}$ ) according to Equation 3.

The above-mentioned results helped design Si doping at the Al sites. The evolution of Si in the cubic  $\alpha-Al_{114}Fe_{24}$  with high stability starts from Si replacements at the Al4 sites to 5/12 occupation with its minimum energy, then Si atoms were added to Al3 sites and then Al7 sites. The relation between the formation energy and Si content at the mixed Al4, Al3 and Al7 sites is shown in Figure 1a. The most stable configuration has a full Si occupation of the Al7 sites and partial occupation of Al3 and Al4 sites and in total 14 Si atoms in the cell, or  $x(Si) = 0.1228$  with  $\Delta E_{Si} = -1.275\text{eV/cell}$  (or  $-53\text{meV/Fe}$  in Figure 1a). Figure 1 revealed a shallow potential well between  $x = 0.10$  to  $0.15$  in  $\alpha-(Al_{1-x}Si_x)_{114}Fe_{24}$  or  $\alpha-(Al_{1-x}Si_x)_{4.75}Fe$ , which indicates flexibility of the chemical composition range. A schematic structure of  $\alpha-(Al_{0.8772}Si_{0.1228})_{4.75}Fe$  is shown in Figure 1b. This model provided the Si distribution at the specific Al sites and updated the experimental model [30].

The partial occupation of Si at the Al3 and Al4 sites means extra freedom in the cubic  $\alpha-(Al_{1-x}Si_x)_{4.75}Fe$  phase. Furthermore, the rather shallow potential well indicates flexibility of this structure. Therefore, one expects a broad range of Si contents in the samples prepared or manufactured at high temperatures, typically over 1000 K, depending on the local chemical environment.

### 3.3. Si Stabilizing the Hexagonal $\alpha'$ -AlFe Phase

The crystal structure of the hexagonal  $\alpha'$ -AlFeSi phase has been investigated intensively [31,32,58,59]. Corby and Black [31] in 1977 reported the detailed structure of  $\alpha'$ -AlFeSi based on the anomalous-dispersion methods from the single-crystal X-ray diffraction pattern. Its lattice was determined to be hexagonal with space group  $P6_3/mmc$  (194). The structure exhibits a complex nature with 23 crystallographically different atomic species: five Fe species and eighteen Al species. Among the five Fe species three are at 12k sites (Fe1, Fe2, Fe3), one at 6h (Fe4) and one at 4f (Fe5). All the iron sites are fully occupied within the errors of the measurements. Among the eighteen Al species, fifteen of them are almost fully occupied and three of them are partially occupied (Table S-1). Recently, Roger *et al.*, revisited this phase using single-crystal X-ray diffraction approach with chemical formula  $Al_{7.1}SiFe_2$ [32]. They also identified the Si sites: Si1 at 12k (Al4 sites according to our note), Si2 at 6h (Al17 sites here) and Si3 at 2c sites (Al18 sites here). Both Si2 and Si3 are mixed with Al atoms: Si2 (Al17) has mixture with a large Si occupation (0.85) with a small Al occupation of 0.15 (Al17).

Meanwhile, Si3 (Al18) has a moderate occupation of 0.14 [32]. The experimental result provided the start point for investigating the Si stabilisation effect in the hexagonal  $\alpha'$ -AlFe phase.

The calculated formations for the configurations of the binary  $\alpha'$ -AlFe phase were shown in Table 1. We chose Config-2 in Table 1 to investigate the Si stabilization effect in this phase, considering the low occupation rate of Al(Si) at the Al18 or Si3 sites [31,32]. The calculated relationship between the formation energy and Si content according to Equation 3 is shown in Figure 2a.

The Si atoms were first added to the Al4 sites which is Si1 in [32]. The configuration with one Si atom at Al4 has a negative formation energy (-0.47eV/cell or -0.01eV/Fe). The full Si occupation of the Al4 sites ( $x(\text{Si1}) = 0.0625$ ) caused a formation energy of -93meV/Fe as shown in Figure 2a. Then six Si atoms were used to replace the Al14 sites (Si2 sites) ( $x(\text{Si1+Si2}) = 0.09375$ ) and the formation energy became -131meV/Fe. Further doping Si at the 6h (Al17) or Si3 sites in [32] lowers down the formation energy till five of the Al atoms were replaced with  $x(\text{Si}) = 0.1198$  and the formation energy is calculated to be -179meV/Fe. Interestingly, adding another Si at the Al17 sites to have a full occupation of the sites raised up the formation energy to -116meV/Fe. Thus, the present calculations provided  $x(\text{Si}) = 0.1198$  in  $(\text{Al}_{1-x}\text{Si}_x)_{192}\text{Fe}_{46}$  is slightly than that  $x(\text{Si}) = 0.1235$  in the formula  $\text{Al}_{7.1}\text{SiFe}_2$  [32]. The slightly higher Si content in the experiment may origin from the partial occupation of the 2c (Al18[31] or Si3[32]) sites and kinetic factors at the formation temperature. Meanwhile, our calculations provided Si occupation of 5/6 at the Al17 sites, which is in good agreement with the experimental observation of a Si occupation of 0.85 [32].

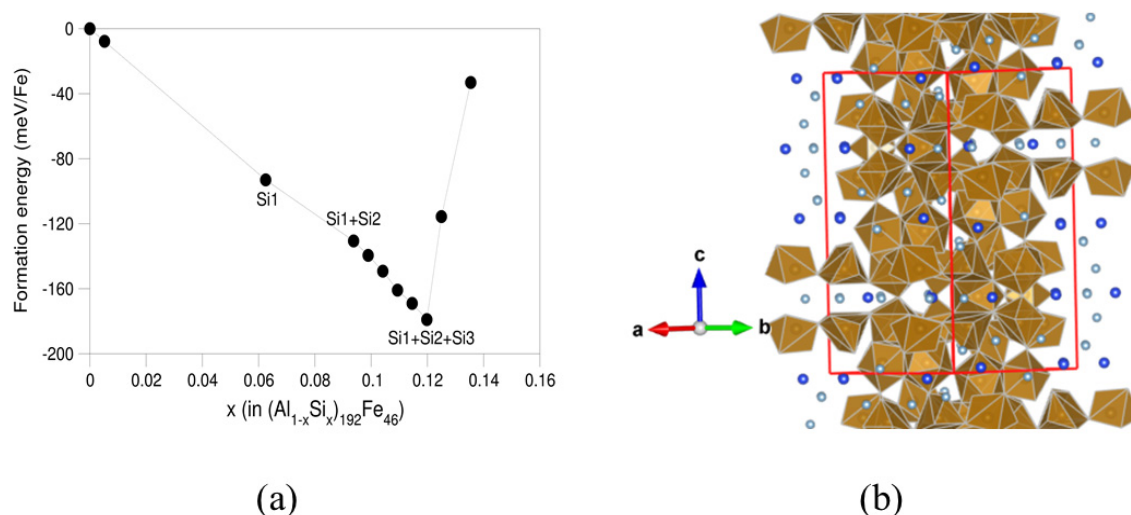


**Figure 2.** (a) The calculated relation between the formation energy and Si content for the highly stable configurations of  $\alpha'$ - $(\text{Al}_{1-x}\text{Si}_x)_{192}\text{Fe}_{46}$  ( $\Delta E_{\text{Si2}}$ ) according to Equation 3. (b) The schematic structure for the most stable configuration with  $x = 0.1198$ . The dotted line in (a) is to guide readers' eyes. The red lines in (b) illustrate the unit cell with the axis shown in the left.

Overall, the present *ab initio* study produced a rather sharp potential well for the Si solution at the specific Al sites (full replacement at the Al4, Al14 and partial replacement at Al17). The most stable structure has the chemical formula  $(\text{Al}_{0.8802}\text{Si}_{0.1198})_{192}\text{Fe}_{46}$  or  $(\text{Al}_{0.8802}\text{Si}_{0.1198})_{4.174}\text{Fe}$ . This study has confirmed the experimental result with consideration of the extra freedom for the Si at the experimental results [32]. The calculations revealed notably significant Si stabilization effect on the hexagonal phase with  $\Delta E_{\text{Si2}} = -179\text{meV/Fe}$  compared with that in the cubic phase (-53meV/Fe).

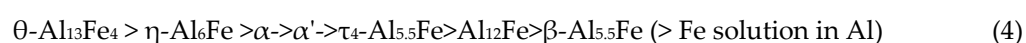
### 3.4. Si Stabilization Effects on the Al-Rich Binary Fe-IMCs

In the Al-rich part of the binary Al-Fe phase diagram [2,36,60] there are a series of Fe-IMCs. Wolverton and Ozolins [36] investigated several Fe-IMCs including  $(\theta)\text{Al}_{13}\text{Fe}_4$  and  $(\eta)\text{Al}_6\text{Fe}$  with the  $\text{Al}_6\text{Mn}$ -type structure. In the last years the frequently observed Al-rich binary and the related

ternary Fe-IMCs including  $\eta$ -Al<sub>6</sub>Fe [44],  $\tau_4$ -(Al,Si)<sub>5</sub>Fe [46],  $\beta$ -Al<sub>4.5</sub>SiFe [45] and  $\theta$ -(Al,Si)<sub>13</sub>Fe<sub>4</sub> [47,48] were investigated. Here we revisited these compounds here together with the above-mentioned cubic  $\alpha$ - and hexagonal  $\alpha'$ -AlFe(Si) phases in a systematic way. A novel phase, Al<sub>12</sub>Fe which is assumed to have the Al<sub>12</sub>Mn type structure [61] was also investigated. The obtained relations between the formation energies and Fe contents for the binary and ternary Fe-IMCs are plotted in Figure 3. The results (calculated lattice parameters and formation energies) of these Fe-IMCs are listed in Table 3.

The calculations showed that dilute solution of an iron atom in Al matrix gains energy with the formation energy ( $\Delta E_f = -0.45\text{eV/Fe}$ , Table 1). Meanwhile solution of a Si atom in Al matrix costs energy ( $\Delta E_f = +0.43\text{eV/Si}$ ). The calculations also revealed that formation of a Si-Fe pair in Al matrix costs about  $0.36\text{eV(Fe-Si)}$ , being lower than that of pure Si solution.

The present investigation on the stability and Si stabilization effects on  $\alpha'$ - vs.  $\alpha$ - represents Si changes the ordering in solidification on the chemical environments. As shown in Figure 3, the relative stability of the binary Fe-IMCs has the series (from high stability (with low formation energy) to low stability (high formation energy) as,



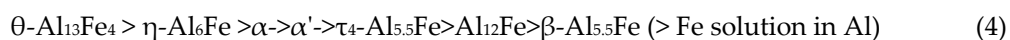
The top three stable binary compounds are  $\theta$ -Al<sub>13</sub>Fe<sub>4</sub> and  $\eta$ -Al<sub>6</sub>Fe and the cubic  $\alpha$ -AlFe. This agrees with the experimental observations that cubic  $\alpha$ -AlFe,  $\theta$ - and  $\eta$ -Al<sub>6</sub>Fe particles are frequently observed in Si-poor conditions [1–4,62].

**Table 3.** The calculated lattice parameters and formation energies with references to the elemental solids via Equation 1 for the frequently observed binary Fe-IMCs and the related ternary Fe-IMCs. Experimental data from the literature were included for comparison. The optimized lattice parameters for  $\alpha(\text{Al}_{0.8772}\text{Si}_{0.1228})_{4.75}\text{Fe}$ ,  $\alpha'(\text{Al}_{0.8802}\text{Si}_{0.1198})_{4.174}\text{Fe}$  and  $\theta(\text{Al}_{0.949}\text{Si}_{0.051})_{13}\text{Fe}_4$  with broken symmetry are the averaged values as they differ moderately from the ones with symmetry.

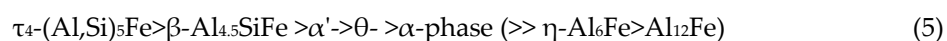
Binary, Fe_IMCs				Ternary Fe-IMCs			
Phase	Latt. S.G.	Paras.(Å)	$\Delta E_f$ (eV/Fe)	Phase	Latt.S.G.	Paras.(Å)	$\Delta E_f$ (eV/Fe)
Al <sub>12</sub> Fe	Cubic Im-3(204)	$a=7.464$	-1.19	-	-	-	-
$\eta$ -Al <sub>6</sub> Fe	Orth. Cmcm(63)	$a=6.465(6.492)[24]$ $b=7.420(7.437)$ $c=8.795(8.788)$	-1.38	-	-	-	-
$\tau_4$ -Al <sub>5</sub> Fe	Tetr. I4/mcm(140)	$l=6.262(-)$ $b=6.262(-)$ $c=9.625(-)$	-1.09	$\tau_4$ -Al <sub>3</sub> Si <sub>2</sub> Fe	Orth. Pbcn(60)	$a=6.057(6.061)[26]$ $b=6.061(6.061)$ $c=9.483(9.525)$	-1.554
$\beta$ -Al <sub>5.5</sub> Fe	Monic. A2/a(15)	$a=6.240(-)$ $b=6.240(-)$ $c=21.087(-)$ $\beta=90.34^\circ(-)$	-1.27	$\beta$ -Al <sub>4.5</sub> SiFe	Monic. A2/a(15)	$a=6.165(6.161)[28]$ $b=6.165(6.175)$ $c=20.766(20.813)$ $\beta=91.43^\circ(90.42^\circ)$	-1.531
$\alpha$ -Al <sub>4.75</sub> Fe	Cubic Pm-3(200)	$a=12.622(12.56)[30]$	-1.32	$\alpha(\text{Al}_{0.8772}\text{Si}_{0.1228})_{4.75}\text{Fe}$	Tricl. P-1(2)	$a=12.534(12.56)[30]$	-1.369
$\alpha'$ -Al <sub>4.174</sub> Fe	Hex. P6 <sub>3</sub> /mmc(194)	$a=12.447(-)$ $c=26.370(-)$	-1.29	$\alpha'(\text{Al}_{0.8802}\text{Si}_{0.1198})_{4.174}\text{Fe}$	Tricl. P-1(2)	$a=12.347(12.345)[32]$ $c=26.222(26.210)$	-1.468
$\theta$ -Al <sub>13</sub> Fe <sub>4</sub>	Monoc. C2/m(12)	$a=15.426(15.492)[33]$ $b=8.022(8.078)$ $c=12.425(12.471)$ $\beta=107.68^\circ(107.69^\circ)$	-1.401	$\theta(\text{Al}_{0.949}\text{Si}_{0.051})_{13}\text{Fe}_4$	Tricl. P-1(2)	$a=15.380(15.492)[33]$ $b=8.012(8.078)$ $c=12.343(12.471)$ $\beta=107.62^\circ(107.69^\circ)$	-1.406

The calculations showed that dilute solution of an iron atom in Al matrix gains energy with the formation energy ( $\Delta E_f = -0.45\text{eV/Fe}$ , Table 1). Meanwhile solution of a Si atom in Al matrix costs energy ( $\Delta E_f = +0.43\text{eV/Si}$ ). The calculations also revealed that formation of a Si-Fe pair in Al matrix costs about  $0.36\text{eV(Fe-Si)}$ , being lower than that of pure Si solution.

The present investigation on the stability and Si stabilisation effects on  $\alpha'$ - vs.  $\alpha$ - represents Si changes the ordering in solidification on the chemical environments. As shown in Figure 3, the relative stability of the binary Fe-IMCs has the series (from high stability (with low formation energy) to low stability (high formation energy) as,



The top three stable binary compounds are  $\theta\text{-Al}_{13}\text{Fe}_4$  and  $\eta\text{-Al}_6\text{Fe}$  and the cubic  $\alpha\text{-AlFe}$ . This agrees with the experimental observations that cubic  $\alpha\text{-AlFe}$ ,  $\theta$ - and  $\eta\text{-Al}_6\text{Fe}$  particles are frequently observed in Si-poor conditions [1–4,62]. This study revealed that Si solution in these compounds has different effects on their stability. For the binary Fe-IMCs with low Fe contents,  $\text{Al}_{12}\text{Fe}$  and  $\eta\text{-Al}_6\text{Fe}$ , Si solution at the Al sites costs energies. The calculations also revealed strong Si stabilization effects on the  $\tau_4$ - and the  $\beta$ -phase and moderate Si stabilization effects on the  $\alpha$ - and the  $\theta$ -phase. It is noted that Si solution stabilized the hexagonal  $\alpha'$ -phase much stronger than on the  $\alpha$ -phase. The results cause change of the stability series of the ternary Fe-IMCs as compared with the binary ones. For the Al-rich ternary Fe-IMCs the stability series is,



The top three compounds of high stability in Al-Fe-Si system are  $\tau_4\text{-(Al,Si)}_5\text{Fe}$ ,  $\beta\text{-Al}_{4.5}\text{SiFe}$  and the hexagonal  $\alpha'$ -phase, which differs notably from that in the binary series (Equation 4). The notably different stability series in Equations 4 and 5 is reflected in the formation of the Fe-IMCs during casting of Al metals with different contents of Si.

#### 4. Discussion

The present calculations revealed stability of the binary Fe-IMCs at 0K in Equation 3. The most stable three Fe-IMCs are  $\theta\text{-Al}_{13}\text{Fe}_4 > \eta\text{-Al}_6\text{Fe} > \alpha\text{-Al}_{4.75}\text{Fe}$ , indicating formation predominance of these compounds during casting in Si-poor Al metals. The predicted results in Equation 3 agree with the experimental observations [1–3,19,49,62,63] that  $\theta\text{-Al}_{13}\text{Fe}_4$ ,  $\eta\text{-Al}_6\text{Fe}$  with some Mn/Fe mixture and  $\alpha\text{-Al}_{4.75}\text{Fe}$  particles are formed and observed as primary intermetallic compounds in Si-poor conditions. Meanwhile, in Si-rich Al alloys, the Fe-IMCs of highest stability are  $\tau_4\text{-(Al,Si)}_5\text{Fe} > \beta\text{-Al}_{4.5}\text{SiFe} > \alpha'$ -phase, which agrees with the experimental observations.

The present work provides an opportunity to discuss the impacts of Si content on the formation of Fe-IMCs during solidification and thermal treatment of Al alloys. Here we first address the Si influences on the  $\alpha$ - and  $\alpha'$ -phases as example.

As shown in Table 3, the content of Si solution in cubic  $\alpha\text{-AlFe}$  phase ( $x \approx 0.122$  in  $(\text{Al}_{1-x}\text{Si}_x)_{4.75}\text{Fe}$ ) is close to that in the hexagonal  $\alpha'$ -phase ( $x \approx 0.120$  in  $\alpha'\text{-(Al}_{1-x}\text{Si}_x)_{4.174}\text{Fe}$ ). Moreover, there are partial Si occupations at some Al sites, which means that the system symmetry has been broken in both crystals (Table 3). A careful analysis of the *ab initio* investigations produced the following diverse results:

i) Si stabilization effect varies with moderate effect on cubic  $\alpha$ -phase ( $\Delta E_{\text{Si2}} = -0.054\text{eV/Fe}$ ) and strong impact on the hexagonal  $\alpha$ -phase ( $\Delta E_{\text{Si2}} = -0.181\text{eV/Fe}$ ).

ii) The compositional flexibility is different in the two phases: A shallow potential valley between  $x = 0.10$  to  $0.15$  for the cubic  $\alpha\text{-(Al}_{1-x}\text{Si}_x)_{4.75}\text{Fe}$  crystal, indicating high flexibility of the chemical composition. Whereas there is a sharp energy well in the energy/Si content relation, indicating rigidity of its chemical composition for  $\alpha'$ -phase.

iii). There are different degrees of extra freedoms caused by the Si partial occupation at the specific Al sites in the two phases. For the cubic  $\alpha\text{-(Al}_{1-x}\text{Si}_x)_{4.75}\text{Fe}$  phase, the most stable configuration contains partial occupation of Al3 (12j) and Al4 (12j) sites (eight Si at the 24 Al positions, see Section 3B), representing number of independent configurations,  $w = [(12 \times 11 \times 10 \times 9) / (4 \times 3 \times 2 \times 1)] \times [(12 \times 11 \times 10 \times 9) / (4 \times 3 \times 2 \times 1)] = 245,024$ . This indicates configurational entropy contributions,  $S_{\text{conf}} = R \ln w = 8.617 \times 10^{-5} (\text{eV/K}) \times 12.409 = 1.07 \times 10^{-3} (\text{eV/K})$  per cell and  $TS_{\text{conf}} = 1.07\text{eV/cell}$  or  $0.045\text{eV/Fe}$  at 1000K. Meanwhile, in  $\alpha'\text{-(Al}_{1-x}\text{Si}_x)_{4.174}\text{Fe}$ , only Si at Al17 (6h sites) has occupation (5/6), which gives  $w = 6$  and

consequently  $S_{\text{conf}} = R \ln w = 8.617 \times 10^{-5} \text{ (eV/K)} \times 1.792 = 0.154 \times 10^{-3} \text{ (eV/K)}$  per cell and  $TS_{\text{conf}} = 0.154 \text{ eV/cell}$  or  $0.003 \text{ eV/Fe}$  at  $1000 \text{ K}$ .

Overall, according to the Gibbs law,  $\Delta G = \Delta H - T \Delta S = -1.369 - 0.045 = -1.414 \text{ eV/Fe}$  for the cubic phase and  $\Delta G = \Delta H - T \Delta S = -1.468 - 0.003 = -1.471 \text{ eV/Fe}$  for the hexagonal phase at  $1000 \text{ K}$ , respectively. These estimations suggested that at the casting conditions, the hexagonal phase is still more stable than the cubic phase at high Si conditions.

Table 3 showed that the Si stabilization effect on the binary Fe-IMCs relates to the Si content in the ternary ones. The related formation energy differences due to Si addition according to Equation 3 are shown in Figure 4.

Figure 4 shows the formation energies due to Si joining at the Al sites decrease with increasing Si content. This relation between formation of Fe-IMCs and Si contents helps understand the formation mechanisms of Fe-IMCs during solidification and thermal treatments of Al alloys with different Si contents.

Formation of Fe-IMCs during casting is a complex process and it depends on the thermodynamics and kinetical factors, as well as compositional and structural templates [2–4,19,49,62,63]. The present study provided thermal properties including formation energies (enthalpies) and configurational contributions of the Fe-IMCs. Meanwhile, other kinetic factors, such as temperature, cooling rates as well as local impurities and their compositions due to inhomogeneity and local structures also play crucial roles in the formation of Fe-IMCs.

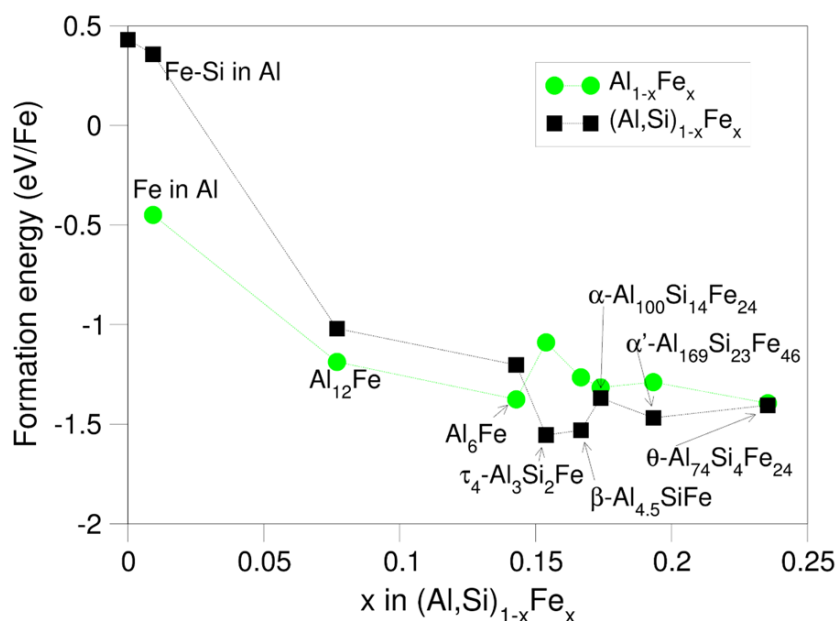


**Figure 4.** Dependence of formation energy,  $\Delta E_{\text{Si2}}$  on the Si content in the ternary Fe-IMCs according to Equation 3. The dotted dark-green line is used to illustrate a linear relation. The Si un-stabilization effects on  $\text{Al}_{12}\text{Fe}$  and  $\eta\text{-Al}_6\text{Fe}$  are not shown.

In practice, Al metals/alloys, particularly those from scraps and waste contain more impurities including other 3d and 4d/5d transition metals beyond the well-known Fe and Si. These transition metal elements may replace Fe to form multiple transition metal alloys with huge numbers of extra freedoms (high-entropy contributions), which may change not only the formation of the Fe-IMCs but also the Si co-joining [14,19,40,42,44,64]. This topic deserves comprehensive investigations particularly the competences among the Fe-IMCs phases.

## 5. Conclusions

The Si stabilization effects on the binary cubic  $\alpha$ - and ternary  $\alpha'$ -AlFe phases were investigated using the first-principles DFT method. The study revealed Si addition changed the relative stability of the two phases that Si stabilizes strongly the hexagonal  $\alpha'$ -phase and moderately the cubic  $\alpha$ -phase. Consequently, the cubic  $\alpha$ -particles are more likely formed in Si-poor conditions while the hexagonal phase in Si-rich Al alloys.

A systematic study on the frequently observed Fe-IMCs revealed that for Si-poor Al alloys, the order series of stability is  $\theta$ -Al<sub>13</sub>Fe<sub>4</sub> >  $\eta$ -Al<sub>6</sub>Fe >  $\alpha$ -Al<sub>4.75</sub>Fe (Equation 4). Si addition changed this series. For Si-rich Al metals, the order series of stability becomes  $\tau_4$ -(Al,Si)<sub>5</sub>Fe >  $\beta$ -Al<sub>4.5</sub>SiFe >  $\alpha'$ -(Al,Si)<sub>4.174</sub>Fe (Equation 5). The obtained information here helps not only understand the formation of Fe-IMCs in Al casting and thermal treatment, but design new casting conditions and new Al alloys of desirable properties from e.g. Al scraps/wastes.

**Supplementary Materials:** The following supporting information can be downloaded at the website of this paper posted on Preprints.org.

**Author Contributions:** Conceptualization, Changming Fang; Methodology, Changming Fang; Software, Changming Fang; Validation, Changming Fang; Formal analysis, Changming Fang; Investigation, Changming Fang; Resources, Changming Fang; Data curation, Changming Fang; Writing – original draft, Changming Fang; Writing – review & editing, Changming Fang and Zhongping Que; Visualization, Changming Fang; Supervision, Zhongyun Fan; Project administration, Changming Fang and Zhongping Que; Funding acquisition, Zhongyun Fan.

**Funding:** This research was funded by The Engineering and Physical Sciences Research Council (EPSRC, UK), grant numbers EP/v011804/1 and EP/S005102/1.

**Conflicts of Interest:** The authors declare no conflicts of interest.

## References

1. Mondolfo, L. F. *Aluminum Alloys: Structure and properties*, Butterworths, London (1976).
2. Khalifa, W.; Samuel, F. H.; Gruzleski, J. E. Iron intermetallic phases in the Al corner of the Al-Si-Fe system. *Metal. Mater. Trans. A*, **2003**, *34*, 807-825.
3. Zhang, H. Effect of iron on the microstructure and mechanical properties of Al-Si alloys. *Light Metals*, **2007**, 775–780.
4. Glazoff, M.L.; Khvan, A.; Zolotarevsky, V.S.; Belov, N. A.; Dinsdale, A. *Casting aluminum alloys: their physical and mechanical metallurgy*. Butterworth-Heinemann, 2018.
5. Schlesinger, M. E. *Aluminum recycling*, CRC Press, Boca Raton (2006).
6. Reuter, M. A.; van Schaik, A.; Gutzmer, J.; Bartie, N.; Abadías-Liomas, A. Challenges of the circular economy: A material, Metallurgical, and Product design perspective. *Ann. Rev. Mater. Res.* **2019**, *49*, 253-274.
7. Kotadia, H. R.; Bareker, N.; Khan, M. H.; Ahuir-Torres, J. L.; Das, A. Aluminium recycling: A critical review of iron-bearing intermetallics in alloys. *Mater. Today Sustainability*, **2025**, *30*, 101119.
8. Chen, H.B.; Xie, Y.L.; Tang, P.; Tang, Z.Y.; Liao, C. W.; Pang, R.H. Demystifying the influence of scrap to raw material ratio on the microstructural and mechanical properties of the secondary 7075 aluminum alloy. *Mater. Lett.* **2025**, *382*, 137847.
9. Zhang, L.F.; Gao, J.W.; Nana, L.; Damoah, W.; Robertson, D.G. Removal of iron aluminum: A review. *Mineral Processing & Extractive Metal. Rev.* **2012**, *33*, 99-157.
10. Gaustad, G.; Olivetti, E.; Kirchain, R. Improving aluminum recycling: A survey of sorting and impurity removal technologies. *Resources, Conservation and Recycling* **2012**, *58*, 79-87.
11. Liddicoat, P.V.; Liao, X.-Z.; Zhao, Y. H.; Zhu, Y.T.; Murashkin, M.Y.; Lavernia, E.J.; Valiev, R.Z.; S. P. Ringer, S.P. Nanostructural hierarchy increases the strength of aluminium alloys. *Nat. Commun.* **2010**, *1*, 63.

12. Qin, L.M.; Tang, P.; Meng, S. X. Effect of Ni addition on the microstructure, conductivities and mechanical properties of as-cast Al-Fe alloys. *J. Alloys Compd.* **2024**, *986*, 174160.
13. Warmuzek, M. Chemical composition of the Ni-containing intermetallic phases in the multicomponent Al alloys. *J. Alloys Compd.* **2014**, *604*, 245–252.
14. Cai, Q.; Fang, C.M.; Lordan, E.; Wang, Y.; Chang, I. T. H.; Cantor, B. A novel Al-Si-Ni-Fe near-eutectic alloy for applications at elevated temperatures, *Scr. Mater.* **2023**, *237*, 115707.
15. Chen, S.L. Recycling of Metals: Importance, Processes, and Future Directions, *J. Powder Metall. Mining* **2024**, *13*, 1000441.
16. Raabe, D.; Tasan, C. C.; Olivetti, E. A. Strategies for improving the sustainability of structural metals. *Nature*, **2019**, *575*, 64–74.
17. Zhu, Y.; Cooper, D. R. An optimal reverse material supply chain for US aluminum scrap. *Procedia CIRP* **2019**, *80*, 677–682.
18. Park, S.-W.; Kayani, S. H.; Park, J.-W.; Lee, M.-Y.; Kim, J.H. Mitigating Fe-rich intermetallic embrittlement in Al-Si-Cu-Mg alloys by deformation-assisted semi-solid rolling. *J. Alloys Compd.* **2026**, *1065*, 188238.
19. Que, Z.P.; Wang, Y.; Fan, Z. Formation of the Fe-containing intermetallic compounds during solidification of Al-5Mg-2Si-0.7Mn-1.1Fe alloy. *Metal. Mater. Trans. A* **2018**, *49*, 2173–2181.
20. Taylor, J. Iron-Containing Intermetallic Phases in Al-Si Based Casting Alloys. *Procedia Mater. Sci.* **2012**, *1*, 19–33.
21. Zienert, T.; Leineber, A.; Fabrichnaya, O. Heat capacity of Fe-Al intermetallics: B2- FeAl, FeAl<sub>2</sub>, Fe<sub>2</sub>Al<sub>3</sub> and Fe<sub>4</sub>Al<sub>13</sub>. *J. Alloys Compd.* **2017**, *725*, 848–859.
22. Sundman, B.; Ohnuma, I.; Dupin, N.; Kattner, U.R.; Fries, S.G. An assessment of the entire Al-Fe system including D0(3) ordering. *Acta Mater.* **2009**, *57*, 3896–2908
23. Marker, M.C.J.; Skolyszewska-Kühberger, B.; Effenberger, H. S.; Schmetterer, C.; Richter, K.W. Phase equilibria and structural investigations in the system Al-Fe-Si. *Intermetallics*. **2011**, *19*, 1919–1929.
24. Walford, L.K. The structure of the intermetallic phase FeAl<sub>6</sub>. *Acta Cryst.* **1965**, *18*, 287–291.
25. Pandey, P.K.; Schubert, K. Strukturuntersuchungen in einigen mischungen T-B3-B4 (T = Mn, Fe, Co, Ir, Ni, Pd; B3 = Al, Ga, Tl; B4 = Si, Ge). *J. less-common metals* **1969**, *18*, 175–202.
26. Gueneau, C.; Servant, C.; D'Yvoir, F.; N. Rodier, N. FeAl<sub>3</sub>Si<sub>2</sub>. *Acta Crystallogr. C* **1995**, *51*, 177–179.
27. Carpenter, G.J.; Lepage, Y. Revised cell data for the β-FeSiAl phase in aluminum alloys. *Scripta Metall. Mater.* **1993**, *28*, 733–736.
28. Rømming, C.; Hansen, V.; Gjønnes, J. Crystal structure of β-Al<sub>4.5</sub>FeSi. *Acta Crystallogr. B* **1994**, *50*, 307–312.
29. Hansen, V.; Hauback, B.; Sundberg, M.; Rømming, C.; Gjønnes, J. β-Al<sub>4.5</sub>FeSi, A combined synchrotron powder diffraction, electron diffraction, high-resolution electron microscopy and single-crystal x-ray diffraction study of a faulted structure. *Acta Crystallogr. B* **1998**, *54*, 351–357.
30. Cooper, M. The crystal structure of the ternary alloy α(AlFeSi). *Acta Cryst.* **1967**, *23*, 1106–1107.
31. Corby, R. N.; Black, P.J. The structure of α-(AlFeSi) by anomalous-dispersion methods. *Acta Cryst. B* **1977**, *33*, 3468–3475.
32. Roger, J.; Bosselet, F.; Viala, J.C. X-ray structural analysis and thermal stability studied of the ternary compound α-AlFeSi. *J. solid state chem.* **2011**, *184*, 1120–1128.
33. Grin, J.; Burkhard, U.; Ellner, M.; Peters, K. Refinement of the Fe<sub>4</sub>Al<sub>13</sub> structure and its relationship to the quasihomological homeotypical structures. *Z. Kristallogr.* **1994**, *209*, 479–487.
34. Jones, R. J. Density functional theory: Its origins, rise to prominence, and future. *Rev. Mod. Phys.* **2015**, *87*, 897–923.
35. B. Huang, B.; G. F. von Rudorff, G. F.; von Lilienfeld, O. The central role of density functional theory in the AI age. *Science*. **2023**, *381*, 170–173.
36. Wolverton, C.; Ozolinč, V. First-principles aluminum database: Energetics of binary Al alloys and compounds. *Phys. Rev. B* **2006**, *73*, 114104.
37. Liu, Y.H.; Chong, X.Y.; Jiang, Y.H.; Zhou, R.; Feng, J. Mechanical properties and electronic structures of Fe-Al intermetallic. *Physica B* **2017**, *506*, 1–11.
38. P. Lafaye, P.; M. Duc Vo, M.; J. Jofre, J.; and J.-P. Harvey, J.-P. Investigating the Al/Si mixed site occupation in the β-AlFeSi phase. *Phys. Chem. Chem. Phys.* **2023**, *25*, 20015–20025.

39. Becker, H.; Bulut, N.; Kortus, J.; Leineweber, A.  $\beta$ -Al<sub>4.5</sub>FeSi: Hierarchical crystal and defect structure: Reconciling experimental and theoretical evidence including the influence of Al vs. Si ordering on the crystal structure. *J. Alloys Compd.* **2022**, *911*, 165015.
40. Popčević, P.; Smontara, A.; Ivkov, J.; Wencka, M.; Komelj, M.; Jeglič, P.; Vrtnik, S.; Bohnar, M.; Jaglič, Z.; Baer, B.; Gille, P.; Borrmann, H.; Burkhardt, U.; Grin, Yu.; Dolinšek, J. Anisotropic physical properties of the Al<sub>13</sub>Fe<sub>4</sub> complex intermetallic and its ternary derivative Al<sub>13</sub>(Fe,Ni)<sub>4</sub>. *Phys. Rev. B* **2010**, *81*, 184203.
41. Ma, D. C. Elastic properties of Mn-rich  $\alpha$  intermetallic phase in engineering aluminum alloy: an ab initio study. *J. Applied Phys.* **2018**, *124*, 085109.
42. Zhang, X.Z.; Wang, D.T.; Nagaumi, H.; Zhou, Y. X.; Yu, W.; Chong, X. Y.; Li, X. Z.; Zhang, H.T. Morphology, thermal stability, electron structure and mechanical properties of  $\alpha$ -AlFeMnSi phases with varying Mn/Fe atomic ratios: experimental studies and DFT calculations. *J. Alloys Compd.* **2022**, *25*, 163523.
43. Amirkhanyan, L.; Weissbach, T.; Gruber, T.; Zienert, T.; Fabricznaya, O.; Kortus, J. Thermodynamic investigation of the  $\tau_4$ -Al-Fe-Si intermetallic ternary phase: A density-functional theory study. *J. Alloys Compd.* **2014**, *598*, 137-141.
44. Dinsdale, A.; Fang, C.M.; Que, Z.P.; Fan, Z. Understanding the thermodynamics and crystal structure of complex Fe containing intermetallic phases formed on solidification of Aluminium alloys. *JOM* **2019**, *71*, 1731-1736.
45. Fang, C.M.; Que, Z.P.; Fan, Z. Crystal Chemistry and Electronic Structure of the  $\beta$ -AlFeSi phase from First-Principles. *J. Solid State Chem.* **2021**, *299*, 122199.
46. Fang, C.M.; Que, Z.P.; Fan, Z. Stability, chemical composition, and structural and electronic properties of the intermetallic compound  $\tau_4$ -(Al,Si)<sub>5</sub>Fe. *J. Alloys Compd.* **2025**, *1037*, 182295.
47. Fang, C.M.; Dinsdale, A.; Que, Z.P.; Fan, Z. Intrinsic defects in and electronic properties of  $\theta$ -Al<sub>13</sub>Fe<sub>4</sub>: An ab initio DFT study. *J. Phys. Mater.* **2019**, *2*, 015004.
48. Fang, C.M.; Que, Z.P.; Dinsdale, A.; Fan, Z. Si solution in  $\theta$ -Al<sub>13</sub>Fe<sub>4</sub> from first-principles. *Intermetallics* **2020**, *126*, 106939.
49. Que, Z.P.; Fang, C.M.; Fan, Z. Nucleation competition and phase transformation mechanisms in recycled aluminium alloys: Insights into  $\theta$ -Al<sub>13</sub>Fe<sub>4</sub>, Al<sub>6</sub>(Fe,Mn) and  $\alpha$ -Al<sub>15</sub>(Fe,Mn)<sub>3</sub>Si<sub>2</sub>. *J. Alloys Compd.* **2025**, *1032*, 181130.
50. Kresse, G.; Furthmüller, J. Efficiency of ab-initio total energy calculations for metals and semiconductors using a plane-wave basis set. *Comp. Mater. Sci.* **1996**, *6*, 15-50.
51. Hohenberg, P.; Kohn, W. Inhomogeneous electron gas. *Phys. Rev. B* **1964**, *136*, 864-B871.
52. Blöchl, P.E. Projector augmented-wave method. *Phys. Rev. B* **1994**, *50*, 17953-17978.
53. Perdew, J.P.; Burke, K.; Ernzerhof, M. Generalized gradient approximation made simple. *Phys. Rev. Lett.* **1996**, *77*, 3865-3868.
54. Fang, C.M.; van Huis, M.A.; Sluiter, M.H.F.; Zandbergen, H.W. Stability, structure and electronic properties of  $\gamma$ -Fe<sub>23</sub>C<sub>6</sub> from first-principles theory. *Acta Mater.* **2010**, *58*, 2968.
55. Monkhorst, H.J.; Pack, J.D. Special points for Brillouin-zone integrations. *Phys. Rev. B.* **1976**, *13*, 5188-5192.
56. Arblaster, J. *Selected values of the crystallographic properties of the elements*. ASM International, Materials Park, Ohio, (2018).
57. Pepperhoff, W.; Acet, M. *The magnetism of iron, in: Constitution and Magnetism of Iron and its Alloys*, Engineering Materials, Springer, Berlin, Heidelberg, (2001).
58. Robinson, K.; Black, P.J. An X-ray examination of  $\alpha$ (Al-Fe-Si) ternary compound. *The London, Edinburgh, and Dublin Philos. Mag. J. Sci.* **1953**, *44*, 1392-1397.
59. Munson, D. A Clarification of the Phases Occurring in Aluminum-Rich Aluminum-Iron-Silicon Alloys with Particular Reference to the Ternary Phase  $\alpha$ -AlFeSi. *J. Inst. Met.* **1967**, *95*, 217-219.
60. Li, X.L.; Scherf, A.; Heilmaier, M.; Stein, F. *The Al-rich part of the Fe-Al phase diagram*. JPEDAV **2016**, *37*, 162-173.
61. Asgar-Khan, M.; Medraj, M. Thermodynamic description of the Mg-Mn, Al-Mn and Mg-Al-Mn systems using the modified quasichemical model for liquid phases. *Mater. Trans.* **2009**, *50*, 1113-1122.

62. Que, Z.P.; Wang, Y.; Mendis, C.L.; Fang, C.M.; Xia, J.H.; Zhou, X.R.; Fan, Z. Understanding of Fe-containing intermetallic compounds in Al-alloys: An overview of advanced in the LiME Research Hub. *Metals* **2022**, *12*, 1677.
63. Shabestari, S.G.; Gruzleski, J.E. The Effect of Solidification Condition and Chemistry on the Formation and Morphology of Complex Intermetallic Compounds in Aluminium—Silicon Alloys. *Cast Metals* **1994**, *6*, 217–224.
64. Baker, I.; Cantor, B.; Yeh, J.W. High Entropy Alloys and Materials. *High Entropy Alloys & Mater.* **2023**, *1*, 1–3.

**Disclaimer/Publisher’s Note:** The statements, opinions and data contained in all publications are solely those of the individual author(s) and contributor(s) and not of MDPI and/or the editor(s). MDPI and/or the editor(s) disclaim responsibility for any injury to people or property resulting from any ideas, methods, instructions or products referred to in the content.